Supporting Information

Gong et al. 10.1073/pnas.1118085109

SI Text

A Model for Phase Transitions in Sea Urchin Spicules. This model simulation was performed using MATLAB and is based on the following hypotheses:

1. The spicule is a two-dimensional matrix of small squares.
2. Before anything is deposited, the color of the small square is black. The color of each small square indicates the type of component [amorphous calcium carbonate (ACC) · H_2O, red; ACC, green; calcite, blue].
3. If there are mixed phases, the color will reflect the mixture of red, green, and blue (RGB), according to the additive color mixing rules.
4. Initially 4,500 small squares are deposited in an oval shape. Additional squares are added at the outer rim of the oval simulating a spicule cross-section growing in girth. The final number of squares is 18,000.
5. Only ACC · H_2O is deposited in the initial oval and at its growing surface.
6. With time, ACC · H_2O gradually transforms into ACC with transition rate a, defined as $[\text{ACC} \cdot H_2O] = e^{-at}$, where $[\text{ACC} \cdot H_2O]$ is the concentration of ACC · H_2O in each small square.
7. With time, ACC gradually transforms into calcite with transition rate b, with the concentration of ACC decaying as $[\text{ACC}] = e^{-bt}$. In the model we assumed $a > b$, thus the ACC · $H_2O \rightarrow$ ACC transition is faster than the ACC $\rightarrow$ calcite transition. (The time t varies between 0 and 100, $a = 0.2$, $b = 0.02$.)
8. If at least one immediately adjacent square is at least 50% calcite, then an ACC square will transform to calcite faster ($b = 0.04$).
9. In the presence of inhibitor, ACC · H_2O will not transform into ACC. The randomly distributed inhibitors are present in only 1% of the pixels, and each inhibitor affects a 3 × 3 pixel region.

The first seven hypotheses are minimal and simply describe how the model works. The sequence of ACC · $H_2O \rightarrow$ ACC $\rightarrow$ calcite transformations assumed in hypotheses 6 and 7 is deduced from the series of spectra in Fig. 2, and supported by the microcalorimetry experiments reported by Radha et al. (1). In hypothesis 7 we assumed $a > b$, so that the ACC · $H_2O \rightarrow$ ACC transition is fast, whereas the ACC $\rightarrow$ calcite transition is slow, for consistency with the observations made in Figs. 2 and 3 that ACC · H_2O is short lived (from a few minutes to a few hours, but not days), and that ACC is longer lived (up to a few days at most, as shown in Fig. S5). Hypothesis 8 is based on secondary nucleation, that is, crystallization of an amorphous phase by contact with an already crystallized phase, as first demonstrated by Killian et al. (2).

Hypothesis 9 is central to the model because it is the crux of what is being tested. Thus in the presence of an inhibitor, ACC · H_2O will not transform into ACC, and the pixels containing it will remain red. We did not simulate the existence of an ACC $\rightarrow$ calcite strong inhibitor because green ACC nanoparticles surrounded by blue calcite were not observed experimentally.

In Fig. S6 we present the results of the model simulations, with and without the ACC · $H_2O \rightarrow$ ACC inhibitor. The two maps are similar in most aspects observed experimentally in Figs. 2, 3, and S5. The existence of ACC · H_2O nanoparticles, red small squares, is observed only when the inhibitor of ACC · $H_2O \rightarrow$ ACC transition is added to the model. The similarity of the model results of Fig. S6 and the experimental results in Figs. 2, 3, and S5 suggests strongly that an inhibitor causes the persistence of ACC · H_2O nanoparticles in the forming spicule.

SI Methods

Extraction of Spicules. Fresh sea urchin spicules were extracted from *Strongylocentrotus purpuratus* embryos, grown in filtered natural sea water containing gentamycin (20 mg L^{-1}) at 15 °C, following established methods (3). Spicules were harvested from late-gastrula stage (36 h postfertilization) embryos, from prism stage (48 h postfertilization) embryos, and pluteus stage (72 h postfertilization) embryos. To isolate the spicules, embryos were first centrifuged at 200 × *g* for 5 min and resuspended in distilled water. The embryos were pelleted at 200 × *g* for 5 min. The pelleted embryos were then resuspended in 10 mM Tris (pH 11) and pelleted again at 200 × *g* for 5 min. The pelleted embryos were resuspended in 10 mM Tris (pH 11) and then disrupted using a Techmar (Polytron style) homogenizer for 1 min at approximately 70% power. SDS was added to the homogenate to a 0.1% (wt/vol) concentration and the resulting mixture was centrifuged at 3,700 × *g* for 5 min. The pellet was resuspended in 10 mM Tris (pH 11) using a glass dounce homogenizer, by a few passes of the pestle. The resuspended pellet was again centrifuged at 3,700 × *g* for 5 min. The pelleted spicules were light brown in color at this stage because they contained cellular debris. The spicules were then washed one more time with 10 mM Tris (pH 11), and then twice with 100% ethanol. The spicules were then gently pelleted and stored on dry ice until they were embedded. We did not use bleach to clean the spicules as is usually done in spicule extraction. We find that the remaining organic material surrounding the spicules is desirable because it greatly improves the stability of ACC · H_2O at the outer rim of spicule cross-sections. At the time of embedding, (within 1–2 h after isolation), the spicules were brought back to room temperature, embedded in epoxy (EpoFix, Electron Microscopy Science). Once cured overnight, the blocks were polished with 50-nm alumina grit (MasterPrep, Buehler). Prior to polishing, the alumina suspension was dialyzed against a 22 g/L solution of Na_2CO_3 in double distilled (DD)-H_2O for 24 h, with three solution changes. This step is important to prevent spicule-ACC dissolution during wet polishing. An ethanol droplet was deposited and let dry on the polished spicule cross-sections, to stabilize the metastable phases (4). The samples were then sputter-coated with 1 nm in the area to be analyzed by X-photoelectron emission spectromicroscopy (PEEM), and 40 nm Pt around it, to provide electrical conductivity to the otherwise insulating crystals (5). All spicules were analyzed by X-ray absorption near-edge structure (XANES)-PEEM within 24 h of extraction from the embryos. The spicule in Fig. S4 was analyzed 4 d and again 2 mo after extraction.

Expression and Isolation of SM50 from *Saccharomyces cerevisiae*. The full-length coding region of the *Strongylocentrotus purpuratus* SM50 gene as well as linker regions at its upstream and downstream ends was generated employing RT-PCR using the One-Step RT-PCR kit from Qiagen. The upstream and downstream primer oligonucleotides used were 5′-GGAATTCCAGCTGACCACCATGAAGGGAGTTTTGTTTATTGTGG-3′ and 5′-CGATCCCCGGGAATTGCCATGTGCCAACGCGTCTGCC-3′. The RNA used was total RNA isolated from *S. purpuratus* 48 h prism stage embryos at a concentration of 0.1 μg/μL. After the full-length SM50 coding region plus linker regions were confirmed correct by DNA sequencing, a region of DNA that

encodes a C terminus tandem affinity purification (TAP) tag (6) was added onto the *SM50* coding region using PCR with the primers 5′-GTATCAACAAAAAATTGTTAATATACCTCTATACTTTAACGTCAAGGAGAAGGAATTCCAGCTGACCACC-3′ and 5′-AGCGGTTGGCTGCTGAGACGGCTATGAAATTCTTTTTCCATCTTCTCTTCGATCCCCGGGAATTGCCATG-3′. The resulting amplicon was then cotransformed into competent *S. cerevisiae* W303 MAT a cells with BamHI- and HindIII-restricted pRSAB1234 plasmid (a gift from Erin K. O'Shea, Harvard University, Cambridge, MA). Transformant colonies were picked and grown up to assay for TAP-SM50 protein expression. A single colony of yeast-expressing TAP-SM50 was picked and a larger scale 2 L culture was grown up to $OD_{600} = 0.6$ at 30 °C, 200 rpm, in synthetic minimal media (ura-) with 2% raffinose as a carbon source and then induced with 2% galatose following standard methods. The induced yeast cells were pelleted and lysed using Y-PER lysis buffer (Thermo Scientific) according to manufacturer's instructions. The resulting soluble fraction of the lysate was mixed with IgG-agarose (Sigma-Aldrich), which bound the soluble TAP-tagged SM50. The resin containing TAP-SM50 was washed extensively with TBS (10 mM Tris, pH 7.5, 100 mM NaCl). SM50 was then released from the resin by digestion with ProTev protease (Promega). The unbound solute was then mixed with a Ni-nitrilotriacetate (NTA)-agarose (Qiagen) to remove the His-tagged ProTev protease. The unbound solute from the Ni-NTA-agarose was collected and dialyzed extensively against deionized water. The resulting sample was then examined by SDS-PAGE and Western blotting techniques using SM50 specific antibodies. The soluble SM50 protein concentration was then adjusted to approximately 0.1 μg/μL and quick-frozen until used.

Extraction of Spicule Matrix Proteins (SMPs). The SMPs used for the in vitro assay of protein functions in Figs. 5 and S7 were extracted from 48 h (prism stage) and 72 h (pluteus stage) *S. purpuratus* embryos as described by Rahda et al. (1). Dry spicules, 1–3 mg, were suspended in approximately 500 μL of dH_2O in 2 mL microfuge tubes. The spicules were demineralized by the gradual dropwise addition of glacial acetic acid while the tubes were kept cold on ice and the suspension thoroughly mixed by trituration. Once the mineral of the spicules was visibly dissolved, the samples were then dialyzed extensively versus dH_2O. Insoluble material was removed from the samples by centrifugation at 15,000 × *g* for 15 min. The SMP samples were then quick-frozen and concentrated using lyophilization. The samples were then adjusted in concentration to 0.3 μg/μL and frozen again until use. There was detectable Ca, when the SMPs were deposited on silicon wafers and analyzed with XANES-PEEM. The mineral form detected was consistently dehydrated-ACC, which we presume is a result of extraction from the spicules or sample preparation, and not from the underlying calcite crystal in the experiment of Fig. S7. In 48 h SMPs there were only trace amounts of Ca, whereas in 72 h SMPs there was much more.

In Vitro Assay Accessing the Stabilization of Calcium Carbonate Mineral Forms. Geologic single crystal calcite wafers 10 mm × 10 mm × 1 mm in size were purchased from MTI Corporation. One-microliter droplets of DD – H_2O or DD – H_2O containing proteins were deposited on the calcite wafers and let dry. Three droplets per wafer were deposited, containing 0.1 μg/μL protein solutions. The proteins were: 48-h SMP and 72-h SMP described above. Cyclin-dependent kinase 1 (cdk1) is a yeast cell cycle protein, which was expressed in *S. cerevisiae*, extracted and purified similarly to SM50, to serve as a control for the protein isolation methods employed here. The other proteins were commercially available, and included: BSA (Sigma-Aldrich), which is not a Ca-binding protein and was chosen to be a nonspecific control; phospholipase A2 (PPL A2), the sea urchin spicule matrix contains a PPL A2 (7), although the one we used here was isolated from honeybee venom (Sigma-Aldrich), and therefore, has a different amino acid sequence.

The dried droplets on calcite were analyzed using the SPHINX microscope. Once an image was obtained and the edge of a droplet identified, stacks of images were acquired across the Ca L-edge, thus each stack contained both calcite wafer and dried droplet pixels, analyzed simultaneously. Pairs of spectra selected from a few pixels in both regions are presented in Figs. 5 and S7.

All proteins measured on calcite with this assay were also measured on Si wafers, to make sure that they did not contain any Ca, none of the single proteins did. The protein mixtures in the 48-h and 72-h SMPs showed a Ca signal in XANES-PEEM analysis. In both cases the mineral form detected was positively identified as dehydrated-ACC, which we presume came from the mineral of the spicules during the isolation of these proteins. In 48-h SMP there were only trace amounts of Ca, whereas in 72-h SMP there was more Ca. The observation of residual ACC from spicules in SMPs is consistent with their in vitro function of stabilizing ACC, as shown in the data of Fig. S7, and consistent with the results of Raz et al. (8).

XANES-PEEM Analysis. Ca mapping was done using the PEEM-3 microscope (9) on beamline 11.0.1 at the Advanced Light Source (ALS) at Lawrence Berkeley National Laboratory, and spectra for the in vitro assay of protein function were done at the Synchrotron Radiation Center (SRC) installed on two different beamlines: the high-energy resolution monochromator (HERMON), and the varied-line spacing plane grating monochromator (VLS-PGM) beamlines. Both beamlines used the SPHINX microscope (10).

For calcium mapping we acquired stacks of 121 images of the same 20-μm field of view, or smaller, with 20-nm pixels, acquired while scanning the photon energy across the Ca L-edge, from 340 to 360 eV, with step 0.1 eV between 345–355 eV, and step 0.5 eV elsewhere. Each pixel in a stack, therefore, contains the full Ca-L-edge spectrum. All spicule spectra were acquired using circularly polarized X-rays to eliminate any possible linear dichroism effects.

Reference Spectra. Each reference spectrum (Fig. 1) was obtained by averaging several single-pixel spectra extracted from different stacks, acquired from 36 or 72 h spicules. This procedure was important to eliminate nonstatistical intensity fluctuations, which occur in each stack of images. In Fig. S2 we present all the single-pixel spectra used, along with their average, and the peak-fitted version of the average spectra. Table S1 shows all fit parameters, and provides a quantitative measure of the peaks 2 and 4 enhancement and shift toward lower energy displayed graphically in Fig. S2.

Component Mapping. For the component mapping in Figs. 2, 3, and S5 we used macros developed in the Gilbert Group, called GG Macros, which run in Igor Pro 6.22, and can be downloaded free of charge from ref. 11. Briefly, using these macros we extract a Ca spectrum from each pixel in a stack, and let the software find the best fit of that spectrum using a linear combination of three predetermined spectral components (Fig. 1) and a third order polynomial. We enforce positivity of the spectral components, and allow the spectra to change energy position within a user-specified window, typically less than 1 eV. The result of this fit is a set of three numbers for each pixel, that is, the proportion (between 0 and 1) of each component present in that pixel. Once this analysis is run for the 10^6 pixels in each stack, we produce proportion maps for the three components ($ACC \cdot H_2O$, ACC, or calcite). Thus for each pixel, the sum of proportions in three proportion maps is always 1. All proportion maps presented here were re-

scaled so the pixels in which the Ca spectra have intensity below a user-specified value (30–45 in the case of Figs. 2 and 3, thus eliminating all pixels from epoxy areas) are removed. The higher-Ca-intensity pixels are retained, and their proportion (between 0 and 1) in each of the three proportion maps is rescaled between 0 and 255. We enhanced the brightness of each pixel, so the brightness is maximum in the dominant channel. Specifically, if a pixel has amounts of red (r), green (g) and blue (b), with r, g, and b varying between 0 and 255 in these 8-bit images, we transformed them from [r g b] to [R G B], where

$$R = 255^{*}r/m \qquad G = 255^{*}g/m \qquad B = 255^{*}b/m,$$

where m is the maximum amount among the r, g, and b values in each pixel.

The resulting RGB map is a brightness-enhanced RGB image. All RGB maps presented here were brightness-enhanced.

The three rescaled, brightness-enhanced proportion maps are then saved as .tif files, and loaded as grayscale into Adobe Photoshop, such that the ACC · H_2O proportion map went into the red channel, the ACC map into the green channel, and the calcite map into the blue channel. We then merged the three RGB channels to obtain an RGB map.

We also did 4-component mapping, including a damage component, as described in Fig. S10 caption. The results of 3-component and 4-component RGB maps were indistinguishable to the naked eye, demonstrating that there is no significant damage to the spicule minerals, and that the results of Figs. 2, 3, and S5 cannot be artifacts of radiation damage (see Fig. S10).

The data presented in Table S2 were calculated from the spicule component analysis maps in Fig. 3. Pixel intensities (0–255) were summed for every pixel in a single color channel (Red, Green, and Blue) for each group of spicules.

1. Radha AV, Forbes TZ, Killian CE, Gilbert PUPA, Navrotsky A (2010) Transformation and crystallization energetics of synthetic and biogenic amorphous calcium carbonate. *Proc Natl Acad Sci USA* 107:16438–16443.
2. Killian CE, et al. (2009) The mechanism of calcite coorientation in the sea urchin tooth. *J Am Chem Soc* 131:18404–18409.
3. Foltz KR, Adams NL, Runft LL (2004) Echinoderm eggs and embryos: Procurement and culture. *Methods Cell Biol* 74:40–71.
4. Sand KK, et al. (2010) Binding of ethanol on calcite: The role of the OH bond and its relevance to biomineralization. *Langmuir* 26:15239–15247.
5. De Stasio G, Frazer BH, Gilbert B, Richter KL, Valley JW (2003) Compensation of charging in X-PEEM: A successful test on mineral inclusions in 4.4 Ga old zircon. *Ultramicroscopy* 98:57–62.
6. Puig O, et al. (2001) The tandem affinity purification (TAP) method: A general procedure of protein complex purification. *Methods* 24:218–229.
7. Mann K, Wilt FH, Poustka A (2010) Proteomic analysis of sea urchin (*Strongylocentrotus purpuratus*) spicule matrix. *Proteome Sci* 8:33.
8. Raz S, Hamilton PC, Wilt FH, Weiner S, Addadi L (2003) The transient phase of amorphous calcium carbonate in sea urchin larval spicules: The involvement of proteins and magnesium ion in its formation and stabilization. *Adv Funct Mater* 13:1–8.
9. Gilbert PUPA, et al. (2008) Gradual ordering in red abalone nacre. *J Am Chem Soc* 130:17519–17527.
10. Frazer BH, Girasole M, Wiese LM, Franz T, De Stasio G (2004) Spectromicroscope for the photoelectron imaging of nanostructures with X-rays (SPHINX): Performance in biology, medicine and geology. *Ultramicroscopy* 99:87–94.
11. GG-Macros (2011) http://home.physics.wisc.edu/gilbert/.

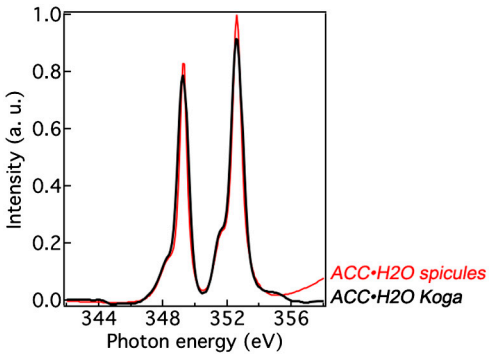

Fig. S1. Comparison of XANES spectra extracted from spicules (red) and from a reference standard compound, ACC · H_2O, prepared with the Koga method (1) (black). The similarity of the two spectra supports our present interpretation, and that of Politi et al. (2) that this amorphous phase in spicules is hydrated ACC. The ACC · H_2O Koga spectrum is from ref. 2, as presented in their figure 1E, top spectrum. The ACC · H_2O spicules spectrum is from this work, and is the result of peak fitting the averaged spectra from six independently acquired 20-nm pixels, as shown in Fig. S2.

1. Koga N, Nakagoe YZ, Tanaka H (1998) Crystallization of amorphous calcium carbonate. *Thermochim Acta* 318:239–244.
2. Politi Y, et al. (2008) Transformation mechanism of amorphous calcium carbonate into calcite in the sea urchin larval spicule. *Proc Natl Acad Sci USA* 105:17362–17366.

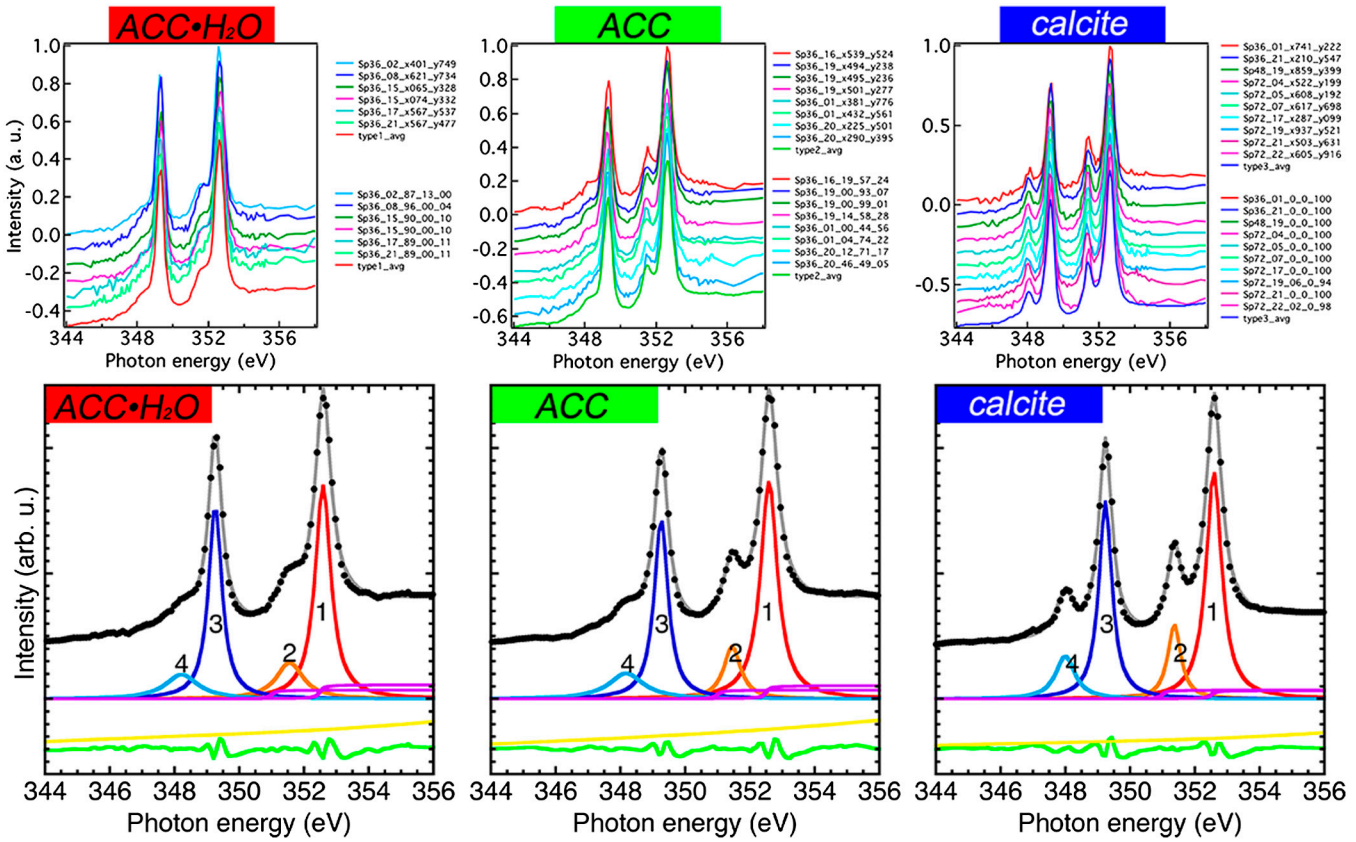

Fig. S2. (*Top*) Averaging and peak fitting of raw spectra to obtain noise-free reference spectra. The top three plots show that for ACC · H_2O, ACC, and calcite we used 6, 8, and 10 raw spectra, respectively, from 20-nm pixels in 36-h, 48-h, or 72-h spicules. Each plot shows two sets of legends corresponding to the same spectra: The top legends show the age of the spicules, the stack number, and the *x* and *y* coordinates of the single pixel from which they were extracted. The bottom set of legends shows spicule age, stack number, and the percentage of ACC · H_2O, ACC, and calcite, respectively, contained in that pixel. For ACC · H_2O and ACC we selected the pixels that gave the greatest ACC · H_2O or ACC percentage, on the order of 90%, in 36-h spicules. For calcite we selected pixels that gave nearly 100% calcite, as most pixels do in 72-h spicules. Each plot shows the average spectrum at the bottom in the red, green, and blue solid lines, respectively. These average spectra were then peak-fitted as shown in the bottom three plots. (*Bottom*) The averaged-spectra data (same as above) are now plotted as black data points, and the fits as solid gray lines. These fits were obtained using four Lorentzian peaks, two arctan, and a third order polynomial. The residues are plotted in green. These are the differences between the experimental data and the results of the peak fitting (black dots and gray lines). The polynomial (yellow) and the residue (green) are displaced down, whereas the data and the fit are displaced up for clarity. All fit components are plotted in different colors. The peak labels 1, 2, 3, 4 are kept at identical positions in all plots to highlight variations in peak intensities and positions. Notice the dramatic increase in the intensity of peak 2 upon dehydration (ACC · H_2O → ACC) and crystallization (ACC → calcite), and of peak 4 upon crystallization (ACC → calcite). There is also a significant shift of peaks 2 and 4 toward lower energies with dehydration and crystallization. See Table S1 for all fit parameters.

Table S1. All fit parameters obtained from the peak-fitting in Figs. 1 and S2

		ACC · H_2O	ACC	Calcite
Background third order polynomial	p0	0.063	0.061	0.033
	p1	0.0057	0.0076	0.0034
	p2	0.00028	0.00028	0.00023
	p3	3.33E-05	1.49E-05	2.73E-05
Lorentzian peak 1	position	352.59	352.59	352.59
	height	0.85	0.87	0.90
	width	0.59	0.64	0.58
Lorentzian peak 2	**position**	**351.56**	**351.45**	**351.37**
	height	**0.14**	**0.21**	**0.30**
	width	1.00	0.63	0.48
Lorentzian peak 3	position	349.26	349.26	349.24
	heigth	0.75	0.71	0.79
	width	0.50	0.52	0.49
Lorentzian peak 4	**position**	**348.22**	**348.18**	**348.00**
	height	**0.10**	**0.11**	**0.17**
	width	1.23	1.30	0.72
Ionization potential arctan 1	position	351	351	351
	height	0.04	0.04	0.04
	width	0.2	0.2	0.2

		ACC · H_2O	ACC	Calcite
Ionization potential arctan 2	position	352.5	352.5	352.5
	height	0.06	0.05	0.03
	width	0.2	0.2	0.2

Notice the most relevant changes highlighted in bold. There is a dramatic increase in the intensity of peak 2 with dehydration and crystallization (from 0.14 to 0.21 to 0.30), and an increase of peak 4 intensity with crystallization (0.11 to 0.17). There is also a significant shift of peaks 2 and 4 toward lower energies with both dehydration and crystallization.

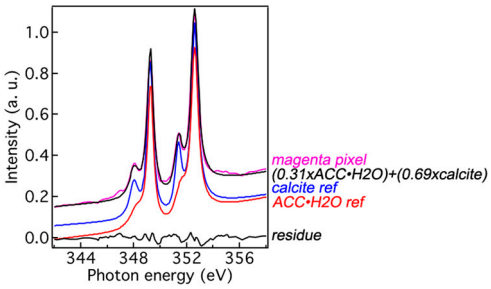

Fig. S3. XANES spectrum (magenta) from one of the magenta 20-nm pixels in Fig. 3. According to the fit results, this portion of the spicule contains 31% ACC · H_2O, no ACC, and 69% calcite. The magenta pixel spectrum is overlapped with a linear-combination-spectrum (black), obtained adding 31% ACC · H_2O spectrum (red) and 69% calcite spectrum (blue). The black and magenta spectra overlap nicely, as demonstrated by the small residue (bottom curve), which is the difference of the two curves, and contains only noise.

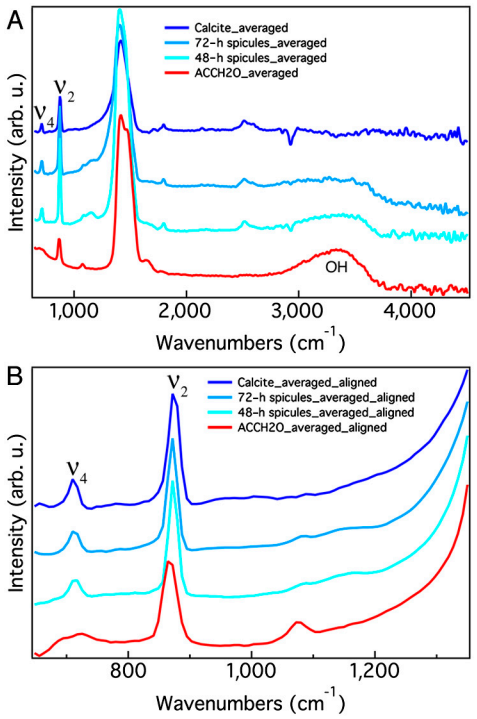

Fig. S4. Attenuated total internal reflection Fourier transform infrared (ATR-FTIR) spectra of 48-h and 72-h fresh spicules, compared to geologic calcite and synthetic ACC · H_2O. (*A*) Full-range ATR-FTIR spectra showing the ν_2 and ν_4 peaks (at 871 cm^{-1} and 711 cm^{-1}, respectively) characteristic of $CaCO_3$, as well as the OH peak characteristic of H_2O. Each spectrum is the average of two or more spectra acquired in different regions of the same sample, and includes many spicules or powder grains. The OH peak shows abundant water in ACC · H_2O (0.017 absorbance units), no water in calcite (0.000), and intermediate water concentrations in 48-h and 72-h spicules (0.009 and 0.008, respectively). (*B*) Same spectra as in *A*, showing only the region of ν_2 and ν_4 peaks. These spectra were aligned in the energy range displayed only, by subtracting the background, that is a third order polynomial fit to each spectrum after masking-off the ν_2 and ν_4 peaks. After this alignment, the intensity ratio of the ν_2 and ν_4 peaks $I(\nu_2)/I(\nu_4)$ is 3.9 for calcite, 5.3 for 72-h spicules, 6.6 for 48-h spicules, and 7.4 for ACC · H_2O. The spectra in both *A* and *B* are displaced vertically for clarity.

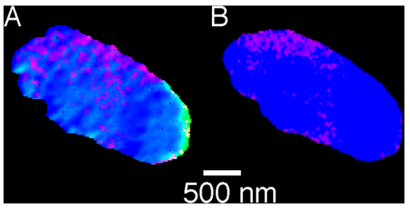

Fig. S5. (*A*) Cross-section of a 48-h (prism stage) sea urchin spicule, imaged and spectroscopically analyzed by XANES-PEEM, 4 d after extraction from the embryo. The pixels are 20 nm. The RGB map is color coded as in Figs. 2 and 3, thus according to additive color mixing (1) red + green = yellow, green + blue = cyan, and red + blue = magenta. Because the red component is present in much lower concentrations, the red level was digitally enhanced, as described in the *SI Methods*, to increase visibility of the magenta nanoparticles. Notice the amorphous phases at the right-hand side edge of the spicule, and the amorphous+crystalline nanoparticles (magenta) inside the spicule cross-section. (*B*) The same spicule in *A*, analyzed again 2 mo later, after storing the sample in a desiccator at room temperature. The ACC at the outer rim had fully crystallized, but magenta nanoparticles persist.

1. Gilbert PUPA, Haeberli W (2011) *Physics in the Arts, Revised Edition*, Complementary Science (Elsevier-Academic, Burlington, MA).

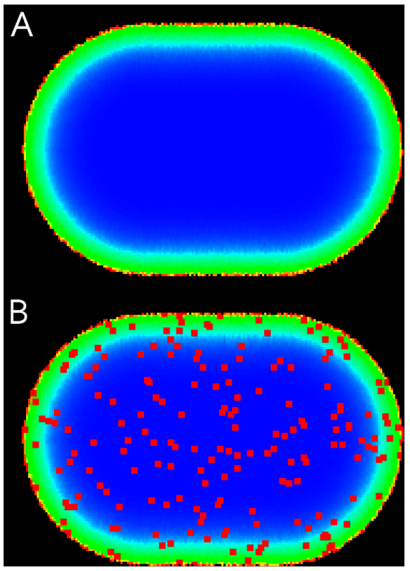

Fig. S6. The RGB maps generated by the model simulation of a forming spicule (*A*) without and (*B*) with an ACC · H_2O → ACC inhibitor. These results correspond to hypotheses 1–8 and 1–9, respectively. In both RGB maps, we note the expected features observed experimentally with XANES-PEEM: red ACC · H_2O exists at the outermost edge of the spicule; immediately inside the outer edge is green ACC; and at the center of the spicule there is mostly calcite. Notice that only the model with inhibitor (*B*) shows ACC · H_2O nanoparticles throughout the model spicule cross-section, as in the experiment of Fig. S5. See animated versions of these model forming spicules in Movies S1 and S2.

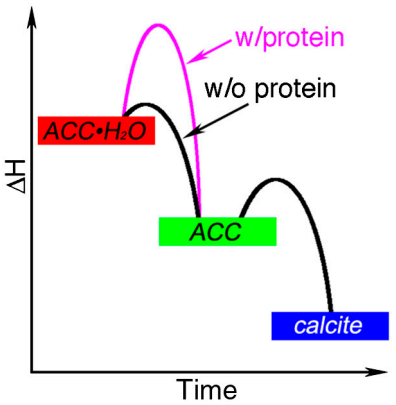

Fig. S7. Proposed energy landscape of the transitions between ACC · H_2O (state at highest, most metastable energy) → ACC → calcite (stable). The relative energy positions are based on the measured values of enthalpy (1). Activation barriers of unknown nature separate the three states. In this schematic representation, the height of each barrier represents a parameter inversely proportional to the transition time. Notice that in the absence of inhibiting protein the activation barrier for ACC · H_2O → ACC is much smaller than for ACC → calcite. In synthetic ACC · H_2O the height of these barriers is reversed (2).

In biogenic ACC, in the presence of inhibiting protein the barrier is much greater (magenta).

1. Radha AV, Forbes TZ, Killian CE, Gilbert PUPA, Navrotsky A (2010) Transformation and crystallization energetics of synthetic and biogenic amorphous calcium carbonate. *Proc Natl Acad Sci USA* 107:16438–16443.
2. Raiteri P, Gale JD (2010) Water is the key to nonclassical nucleation of amorphous calcium carbonate. *J Am Chem Soc* 132:17623–17634.

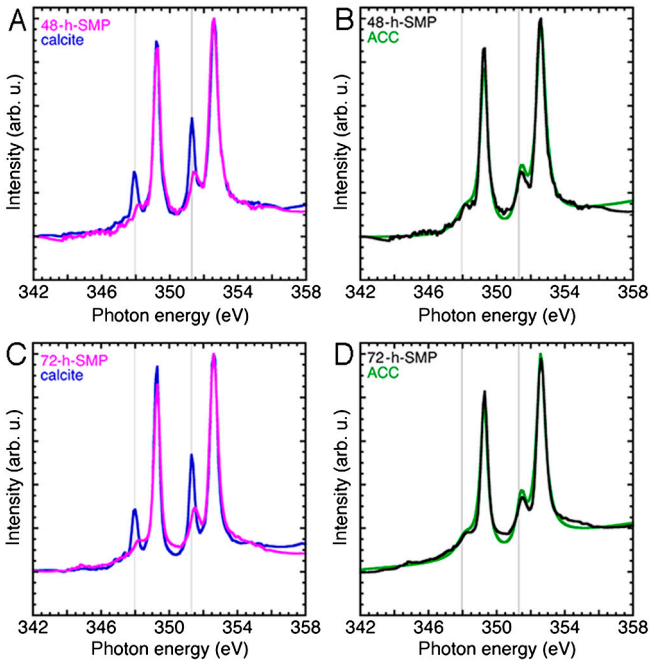

Fig. S8. Additional spectra obtained from the in vitro assay of protein functions described in the text. (*A* and *C*) Integral SMP extracted from 48-h (prism stage) and 72-h (pluteus stage) embryos of *S. purpuratus*. The spectra acquired from 48-h SMP or 72-h SMP dried-droplets on calcite are shown in magenta and compared with calcite (blue). The reprecipitate in the presence of all proteins in the spicule, whether 48 h or 72 h, is clearly not calcite but dehydrated ACC. (*B* and *D*) Comparison of the spectra in *A* and *C* with the reference dehydrated ACC (green).

The spectra are very similar, demonstrating that one or more spicule matrix proteins stabilize anhydrous ACC, even in direct contact with a crystalline calcite wafer. This observation is in agreement with previous experiments by the Addadi–Weiner group (4). ACC stabilization by spicule matrix proteins explains the long-lived ACC phase observed in Fig. S5*A*, although we do not know at present which ones, among the 218 spicule matrix proteins identified by Mann et al. (7) stabilize dehydrated ACC.

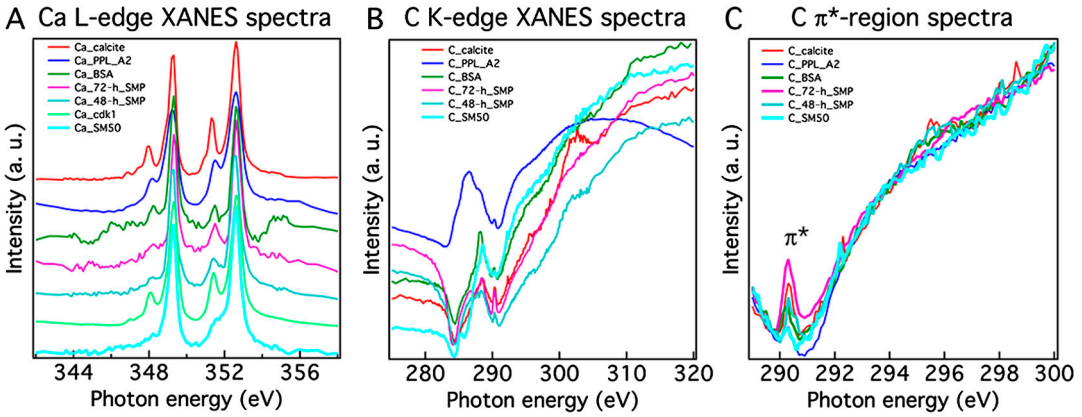

Fig. S9. XANES spectra for all proteins in Figs. 4 and S8, and the calcium L-edge (*A*) and carbon K-edge (*B*, *C*) edges, acquired from the exact same region in each sample. In all cases a region of dried protein droplet on calcite was analyzed. All $CaCO_3$ species, whether amorphous or crystalline, exhibit the carbonate π^* peak in the unnormalized carbon spectra in *B*. The π^* peak at 290.3 eV is magnified in *C*, where the spectral backgrounds were aligned to overlap as much as possible. The C spectrum for cdk1 was not acquired, because the Ca spectrum shows that the reprecipitate is clearly calcite. A technical comment for the spectromicroscopist: The presence of the π^* peak was deemed sufficient to identify the existence of a carbonate cluster. Notice that in the amorphous species (SM50, 48-h SMP, 72-h SMP) the carbonate π^* peak cannot originate from the calcite substrate. If photoelectrons at the carbon π^* originated from the underlying calcite crystal, then in the same exact regions photoelectron at the calcium L-edge would come from even deeper into the crystal because their initial kinetic energy is greater (1). In this case they should show the characteristic calcite crystal field peaks in the Ca spectra, and they clearly do not. Therefore, in both Ca and C spectra the signal originates from reprecipitated carbonates at the surface of the dried protein droplets.

1. Frazer BH, Gilbert B, Sonderegger BR, De Stasio G (2003) The probing depth of total electron yield in the sub keV range: TEY-XAS and X-PEEM. *Surf Sci* 537:161–167.

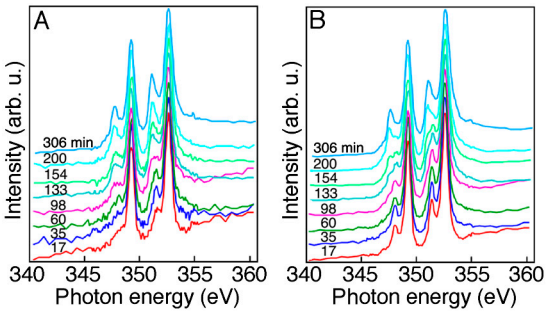

Fig. S10. The effect of radiation damage on Ca spectra from 48-h (prism stage) spicules. (*A*) Single-pixel XANES spectrum from a 20-nm pixel originally containing mostly amorphous phases (53% ACC · H_2O, 35% ACC, and only 7% calcite). The first spectrum at the bottom was acquired with a total exposure time of 17 min. The others were acquired after exposing for the indicated lengths of time, in minutes. (*B*) XANES spectra from a 20-nm pixel originally containing 100% calcite in the 17-min spectrum. Both pixels in *A* and *B*, after long exposure times, show CaO spectra. At shorter exposure times, e.g., 60 min (dark green spectrum in *A*), ACC has effectively transformed into calcite. With increasing time of X-ray beam exposure, ACC · H_2O transforms into ACC, which subsequently transforms into calcite. Calcite then transforms into CaO and CO_2. The effect of radiation damage starts to appear spectroscopically after 35 and 98 min of exposure, respectively, for ACC and calcite pixels. The 306-min spectra in both plots are pure CaO, with no residual calcite. The data of Figs. 2 and 3 were acquired with exposure time of 20 min or less, hence their spectroscopic results should not be affected by radiation damage to carbonates. In addition, we repeated the component mapping in Figs. 2 and 3–48 h using four components. The fourth component is the pure CaO spectrum of the most damaged 306-min spectrum shown here. Only a small percentage of each pixel spectrum contained any CaO, and CaO pixels were usually colocalized with the amorphous phases, indicating their greater sensitivity to damage. ACC · H_2O-rich and ACC-rich pixels always contained <20% CaO, whereas calcite-rich pixels had <1% CaO. A comparison between 3- and 4-component mapping of the spicules in Figs. 2 and 3 did not show qualitative differences. Spectroscopic differences observed here are not due to crystal orientation and linear dichroism effects because we used circularly polarized light to correct for that possibility.

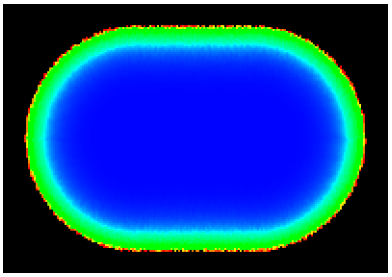

Movie S1. Cross-section of a forming spicule, simulated without any ACC · H_2O → ACC inhibitor. As the spicule grows, more red ACC · H_2O is deposited at the outer rim, and they gradually transforms into green ACC and then into blue calcite. This simulation follows hypotheses 1–8.

Movie S1 (MOV)

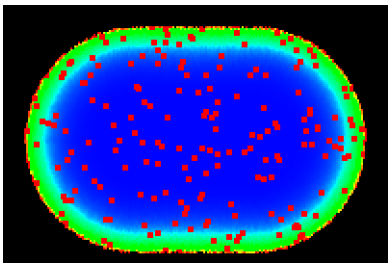

Movie S2. Simulated RGB map of a forming spicule with ACC · H_2O → ACC inhibitor, thus including hypothesis 9: In the presence of inhibitor, ACC · H_2O will not transform into ACC. The randomly distributed inhibitors are present in 1% of the pixels, and each inhibitor affects a 3×3 pixel region. Notice that this simulation shows long-lived ACC · H_2O nanoparticles throughout the model spicule cross-section, as found in the experiment of Fig. S5.

Movie S2 (MOV)

Table S2. Quantitative analysis of ACC · H_2O (red), ACC (green), and calcite (blue) as identified from the Ca spectroscopy and component mapping in all the spicules of Fig. 3

Spicule age (h)	Color channel	Total no. of pixels	Total (%)
36	red	17788188	40
36	green	8538670	20
36	blue	17399907	40
48	red	3967073	9
48	green	15111247	32
48	blue	27237947	59
72	red	427200	1
72	green	20735	0
72	blue	58518089	99

Notice that in 36-h, 48-h, and 72-h spicules the $CaCO_3$ present is 60, 41, and 1% amorphous, whereas 40, 9, and 1% is ACC · H_2O. Regarding water, we stress that the latter results only apparently indicate less water than expected, based on previous analysis (1, 8). Water not in the immediate vicinity of Ca atoms would go undetected in XANES spectra at the Ca edge. Hence these results should be interpreted not as water-content analysis, but as calcium-nearest-neighbor-water analysis. The FTIR data of Fig. S4 yield bulk-water analysis, whether this water is near or far from Ca atoms.